OPEN ACCESS
IOP Publishing
Superconductor Science and Technology
Supercond. Sci. Technol. **33** (2020) 035012 (7pp)
https://doi.org/10.1088/1361-6668/ab6ec1

Sharp-selectivity in-line topology low temperature superconducting bandpass filter for superconducting quantum applications

Yuxing He[1], Shiori Michibayashi[2], Naoki Takeuchi[1] and Nobuyuki Yoshikawa[1,2]

[1] Institute of Advanced Sciences, Yokohama National University, Yokohama 240-8501, Japan
[2] Department of Electrical and Computer Engineering, Yokohama National University, Yokohama 240-8501, Japan, Yokohama 240-8501, Japan

E-mail: he-yuxing-zj@ynu.ac.jp

Received 6 October 2019, revised 15 December 2019
Accepted for publication 22 January 2020
Published 12 February 2020

Abstract

This paper presents a new class of sharp-selectivity low-temperature superconducting filter that incorporates lumped element resonant couplings. Dependent on a novel synthesis approach, the proposed filter exhibits great advantages such as: (1) a very simple in-line topology (without any cross coupling), (2) extremely compact size based on lumped inductor-capacitor (*LC*) elements, and (3) multiple transmission zeros (TZs) independently generated and controlled (via each resonant coupling). To facilitate the physical implementation, a group of lumped element circuit models are detailed, where series *LC* units are adopted for both the resonators and the resonant couplings. Considering an in-line topology here, the entire filter layout is then designed by cascading the lumped models one after another. For verification, a 5th-order bandpass filter centered at 5 GHz, with 500 MHz bandwidth and 3 TZs, is designed, simulated, and tested at cryogenic temperature (4.2 K). Moreover, preliminary simulations of the presented filter in series with an on-chip rapid single-flux-quantum microwave pulse generator are discussed for superconducting quantum applications.

Keywords: superconducting filter, resonant coupling, low-temperature superconductor, quantum computing

(Some figures may appear in colour only in the online journal)

1. Introduction

Microwave filters play an important role in a variety of superconducting analog and digital systems and therefore have attracted much attention in recent years. In [1–4], one very popular topic concerns the design of high-temperature superconducting (HTS) filters based on distributed resonant structures. By replacing normal metal layers with HTS thin-film materials, these filters provide an extremely low insertion-loss performance that is crucially demanded in modern wireless applications.

Recently, low temperature superconducting (LTS) microwave circuits have been extensively investigated for superconducting quantum computing systems [5–9]. Specifically, we have been developing an on-chip rapid single-flux-quantum microwave pulse generator (RSFQ MPG) [10, 11] to control superconducting qubits in a scalable quantum computing system [12]. Figure 1 illustrates the schematic of an RSFQ MPG. The clock (CLK) generator

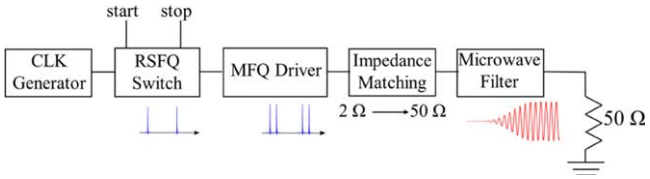

Figure 1. Ideal schematic of a RSFQ MPG, where the filter is a key component to convert an MFQ pulse train to a gradient microwave pulse.

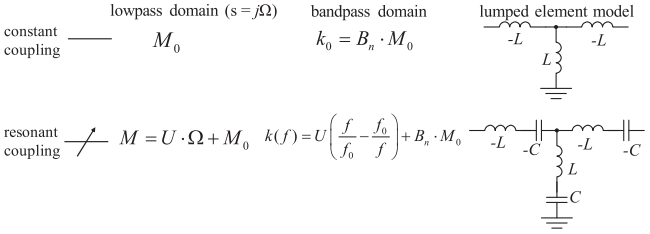

Figure 2. Comparison of the proposed resonant coupling with an established constant coupling [22–24] in the lowpass Ω-domain, bandpass domain, and their equivalent circuit models. Note that f_0 refers to the center frequency, while B_n represents the fractional bandwidth of a bandpass filter.

outputs a single-flux-quantum (SFQ) pulse train, the duration time of which is controlled by the RSFQ switch. Then, the multi-flux-quantum (MFQ) driver converts an SFQ pulse into an MFQ pulse to amplify the final output level. Here, the microwave filter functions as a key component to convert the MFQ pulse train into a microwave pulse, and should satisfy the following requirements: (1) on-chip implementation with extremely compact size, which indicates that lumped *LC* structures are preferred; and (2) sharp frequency selectivity as well as uneven group delay performance, which can control the rise and fall time of the microwave pulse. Especially, for quantum annealing machines using nonlinear oscillators [13–15], it is required to very slowly ramp up microwave pulses because the ramp-up time corresponds to the temperature scheduling.

Relying on the same idea, a group of lumped or quasi-lumped LTS filters are designed and associated with RSFQ circuitry for qubit controls in [16–19]. More efforts, dealing with the implementation techniques of LTS filters, are reported in [20] and [21]. These proposed filters, based on conventional Chebyshev characteristics, however, require a very high order and massive elementary units. Thus, a favorable mechanism to meet the frequency selectivity and group delay performance for our purpose remains a problem.

In this work, we propose a new class of LTS lumped element bandpass filter possessing generalized Chebyshev characteristics [22], where the desired frequency selectivity and group delay requirements are achieved with a small number of transmission zeros (TZs). Note that, without cross coupling (compared with literatures [1–4]), the TZs here are individually generated via *resonant couplings* (also called frequency-variant couplings), figure 2. As a result, the filter can be structured by a simple in-line topology as figure 3 shows, where the configuration simplicity as well as TZ independence are quite beneficial for RSFQ MPG realization.

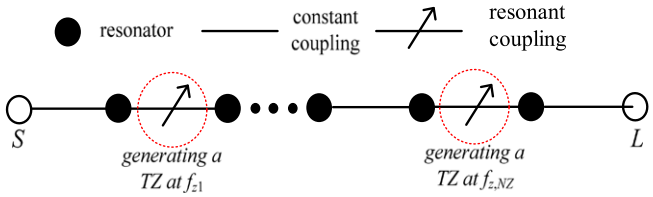

Figure 3. Ideal prototype of an *N*th-order in-line topology filter containing resonant couplings.

In the following, a synthesis theory to determine the presented in-line prototype is described in section 2. Series type *LC* unit models for constructing the resonators and couplings are detailed in section 3. In section 4, a 5th-order bandpass filter, centered at 5 GHz with 10% bandwidth and three finite TZs, is demonstrated for validation. The simulated waveform by utilizing such a filter with an RSFQ MPG is also provided to show its availability for superconducting quantum applications. Finally, section 5 concludes the paper.

2. Synthesis theory

Direct synthesis technique refers to a deterministic procedure to identify the topology as well as all the coupling coefficients of an *N*th-order filter network. This usually involves the admittance matrix transformations of the filter lowpass prototype by [22]

$$[Y_{k+1}] = [T_{k+1}][Y_k][T_{k+1}]^T, \ i = 0, 1, 2, \ldots, K \qquad (1)$$

As a result, undesired couplings from an original prototype (with admittance matrix $[Y_0]$) are annihilated and we finally derive a practical filter topology (with admittance matrix $[Y_{K+1}]$) that is very suitable for physical implementation. By means of diverse synthesis techniques in literature (e.g. [22–24]), a variety of practical topologies comprising cross-coupled constant couplings have been proposed. These topologies provide basic design principles for many filter constructions, such as [1–4].

Particularly, the in-line topology shown in figure 3 is considered as the most attractive solution due to its simplicity; and we have accomplished the relevant synthesis procedure very recently in [25, 26]. Without any cross-coupling involved (e.g., in [1–4]), here the TZs are separately generated via a set of resonant couplings between adjacent resonators. Accordingly, the admittance matrix (named as $[Y_{final}]$) is determined in terms of (1), as figure 4 shows. Note that, $[Y_{final}]$ identifies all the coupling coefficients required for the filter realization. Due to an in-line topology, it is apparent in figure 4 that non-zero coupling coefficients only exist in the diagonal arrows.

3. Lumped element models

To physically realize the derived in-line filter in the bandpass domain, a lumped element transformation technique by applying series *LC* units is introduced in this paper. As a

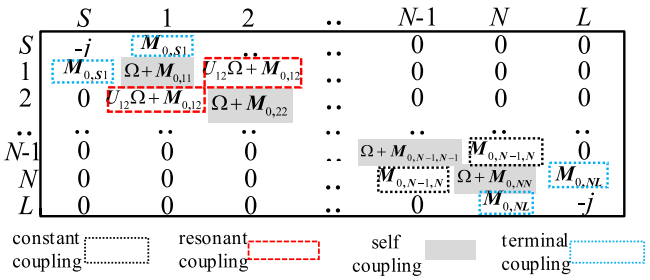

Figure 4. A possible form of the admittance matrix $[Y_{final}]$ for the proposed in-line prototype (in the lowpass domain). Note that four types of couplings (described in [22]) are involved and denoted in different blankets.

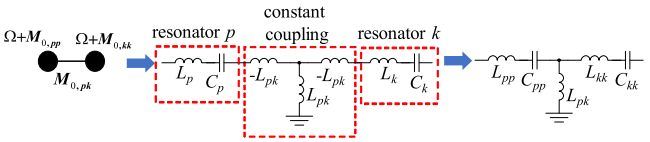

Figure 5. Block A: lumped circuit model for two resonators connected by a constant coupling.

result, all the capacitances and inductances can be obtained at one time. Regarding the prototype in figure 3, here we consider three elementary blocks for the filter construction, i.e., resonators connected by a constant coupling (block A), resonators connected by a resonant coupling (block B), and terminal resonators connected to the source/load (block C). In the following, the fractional bandwidth of the filter in the bandpass domain is assumed as B_n, while the center frequency is f_0. In addition, χ_i ($i = 1, 2 \ldots, N$) gives the reactance-slope parameter of each LC resonator [27], which are manually selected during design.

3.1. Block A: resonators connected by a constant coupling

The lumped model for block A is illustrated in figure 5. Note that two resonators, p and k, are modeled by series LC resonant units separately. Moreover, the constant coupling is realized via a traditional T-shape K-inverter comprising both positive and negative inductances (i.e., L_{pk}) [27], where the negative parameters are thereafter absorbed into the resonators at both sides (see right side of figure 5). The eventual inductances and capacitances of block A are thus obtained as:

$$\begin{aligned} L_{pk} &= \sqrt{\chi_p \chi_k} B_n M_{0,pk} \big/ (2\pi f_0) \\ L_{pp} &= \chi_p \big/ (\pi f_0 (\sqrt{(B_n M_{0,pp})^2 + 4} - B_n M_{0,pp})) - L_{pk} \\ C_{pp} &= C_p = 1 \big/ (\pi f_0 \chi_p (\sqrt{(B_n M_{0,pp})^2 + 4} - B_n M_{0,pp})), \end{aligned} \quad (2)$$

where the coupling coefficients $M_{0,pp}$ and $M_{0,pk}$ are derived from the former section. Accordingly, L_{kk} and C_{kk} can be obtained in the same manner.

3.2. Block B: resonators connected by a resonant coupling

The lumped model for a resonant coupling is however never discussed in the literature. Specifically, here we propose a new kind of K-inverter comprising series LC resonant units,

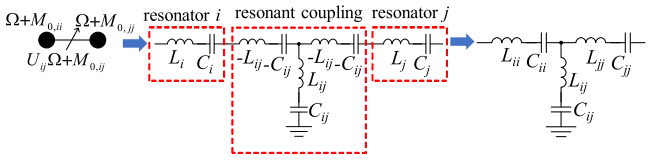

Figure 6. Block B: lumped circuit model for resonators connected by a resonant coupling.

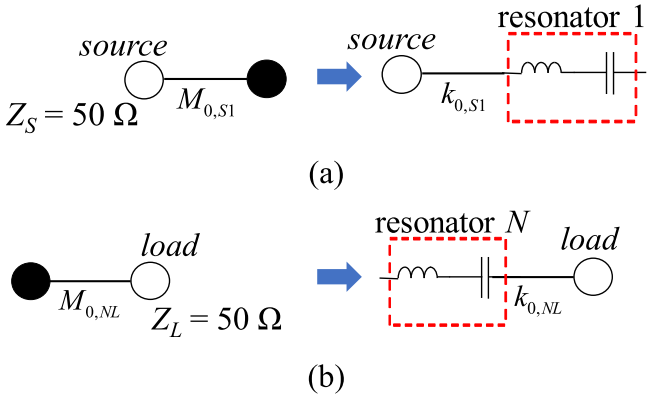

Figure 7. Block C: lumped circuit models for terminal couplings at (a) source and (b) load, respectively. Note that $k_{0,S1}$ and $k_{0,NL}$ are removed in implementation once stipulating χ_1 and χ_N by equation (5).

as shown in figure 6. By absorbing all the negative parameters into the resonators (see right side of figure 6), the ultimate circuit parameters are determined by:

$$\begin{aligned} L_{ij} &= U_{ij} \sqrt{\chi_i \chi_j} \big/ (\pi f_0 (\sqrt{(B_n M_{0,ij}/U_{ij})^2 + 4} - B_n M_{0,ij}/U_{ij})) \\ C_{ij} &= 1 \big/ (\pi f_0 U_{ij} \sqrt{\chi_i \chi_j} (\sqrt{(B_n M_{0,ij}/U_{ij})^2 + 4} - B_n M_{0,ij}/U_{ij})) \\ L_{ii} &= \chi_i \big/ (\pi f_0 (\sqrt{(B_n M_{0,ii})^2 + 4} - B_n M_{0,ii})) - L_{ij} \\ C_{ii} &= 1 \big/ [1 \big/ (\pi f_0 \chi_i (\sqrt{(B_n M_{0,ii})^2 + 4} - B_n M_{0,ii})) - 1/C_{ij}] \end{aligned} \quad (3)$$

3.3. Block C: terminal resonators connected to source/load

On the other hand, the terminal couplings at source and load in figure 7 are processed with a particular mechanism. Considering the source and load impedances as Z_S and Z_L (suppose $Z_S = Z_L = 50\ \Omega$ in this work), respectively, the de-normalized coupling coefficients in the bandpass domain are calculated directly as [28]:

$$k_{0,S1} = M_{0,S1} \sqrt{Z_S B_n \chi_1}, \quad k_{0,NL} = M_{0,NL} \sqrt{Z_L B_n \chi_N} \quad (4)$$

It is then interesting to notice that, by selecting χ_1 and χ_N as

$$\chi_1 = 50 \big/ (B_n M_{0,S1}^2), \quad \chi_N = 50 \big/ (B_n M_{0,NL}^2), \quad (5)$$

the couplings $k_{0,S1}$ and $k_{0,NL}$ will become equal to the 50 Ω terminal impedances. It implies that these terminal couplings

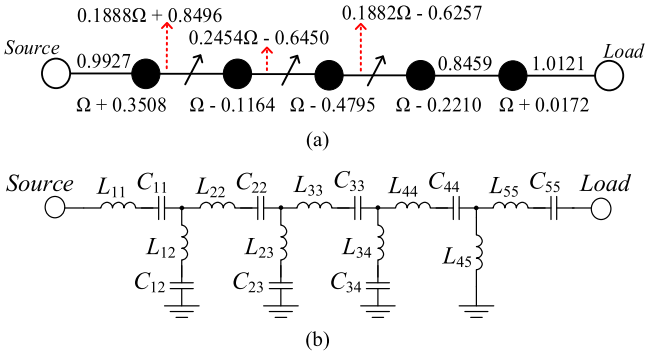

Figure 8. (a) Coupling coefficients of the 5th-order example in the lowpass domain. (b) Resultant lumped element circuit model of the 5th-order example in the bandpass domain.

can be removed without influence on the filter response, which further miniaturizes the whole filter area [29].

4. Experimental example

4.1. Synthesis & parameters extraction

Based on the proposed method, a 5th-order in-line example centered as $f_0 = 5$ GHz, with fractional bandwidth $B_n = 10\%$, 20-dB return loss, containing three TZs at 4.0 GHz, 5.7 GHz, and 5.9 GHz, is demonstrated for the validation. In terms of the synthesis in section 2, the resultant lowpass prototype is derived as figure 8(a) shows, where the 3 TZs (turn into $-4.5j$, $2.628j$, and $3.325j$ in lowpass domain) are corresponded to respective resonant couplings individually. By stipulating the resistance slopes as $\chi_1 = 405.8$, $\chi_2 = 350$, $\chi_3 = 350$, $\chi_4 = 350$, $\chi_5 = 385.3$, the lumped element schematic is then obtained based on (2)–(5) once incorporating blocks A, B, and C together, which is exhibited in figure 8(b). It should be stressed that χ_1 and χ_5 here are specifically decided via (5) to ensure direct connection of source-resonator 1 and load-resonator N without terminal structures, as we presented in section 3.3. The derived inductance and capacitance parameters are listed by the following: $C_{11} = 0.114$ pF, $C_{22} = 0.175$ pF, $C_{33} = 0.187$ pF, $C_{44} = 0.122$ pF, $C_{55} = 0.100$ pF, $L_{11} = 8.34$ nH, $L_{22} = 5.30$ nH, $L_{33} = 6.32$ nH, $L_{44} = 7.60$ nH, $L_{55} = 8.79$ nH, $C_{12} = 0.488$ pF, $C_{23} = 0.300$ pF, $C_{34} = 0.380$ pF, $L_{12} = 3.24$ nH, $L_{23} = 2.61$ nH, $L_{34} = 1.92$ nH, and $L_{45} = 1.13$ nH.

4.2. Physical implementation

The obtained LC network is implemented by using the AIST Nb 2.5 kA cm^{-2} Standard Process 2 (STP2) [30]. Particularly, the inductors are constructed by using spiral coils on M4 layer, and the capacitors are realized by parallel plates on M3 and M4 layers. The relevant layouts are initially determined from a 3D extractor InductEx (v5.06) [31], and then adjusted under ANSYS Electromagnetic Suites (v19.2).

Specifically, figure 9(a) gives the layout view of the L_{11} & C_{11} resonant unit. As the desired lumped parameters are already known in figure 8, the layout can thus be adjusted by fitting its reactance the same with that of the lumped element model, which is illustrated in figure 9(b). The same process is utilized to other sub-networks (e.g., L_{22} & C_{22}, L_{12} & C_{12}, etc) as well.

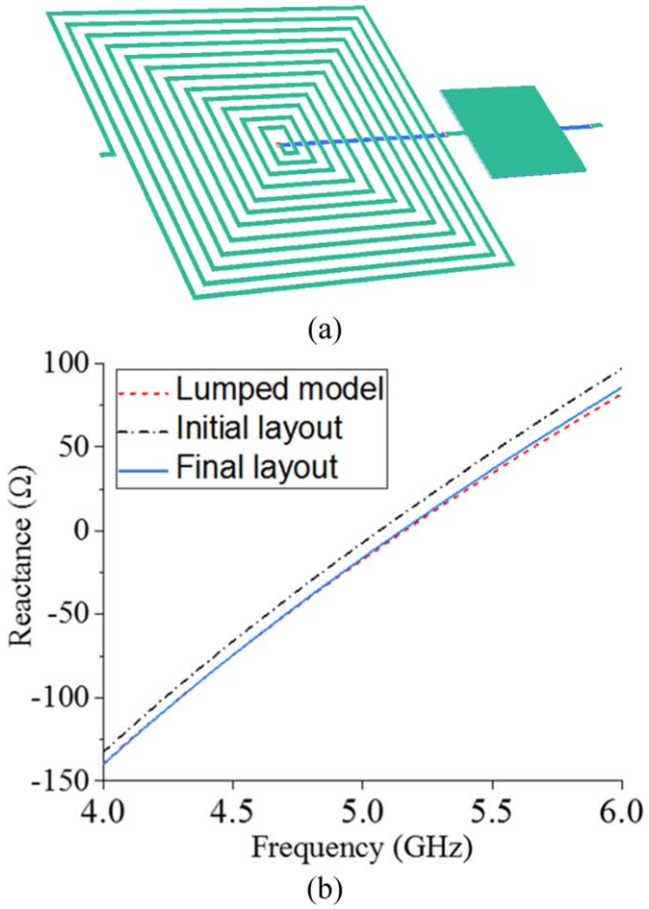

Figure 9. (a) Layout view of resonant unit comprising L_{11} & C_{11}, and (b) its reactance before (black dash dot line) and after (blue solid line) adjustment.

Since an in-line topology is concerned, the whole layout of the 5th-order filter can then be constructed with sub-networks (namely the resonant units) in series. Figure 10 gives the micrograph of the fabricated filter. Note that, an M1 layer is placed outside of the lumped elements to shunt C_{12}, C_{23}, C_{34}, and L_{45} to ground. Note that the total size of the filter is 1650 μm × 350 μm, which is 53% reduced from our previous lowpass filter designed in [11].

4.3. Experimental results

The filter is then measured by a vector network analyzer (Keysight, P9374A) at a 4.2 K cryogenic temperature. The tested result is compared with EM simulation in figure 11. Imperfection of in-band return loss and insertion loss are mainly attributed to the frequency response of the cryogenic probe during measurement. Nevertheless, a sharp out-of-band selectivity (with 3 TZs at almost desired locations) can be obtained in both simulation and measurement, therefore revealing the validity of the presented approach.

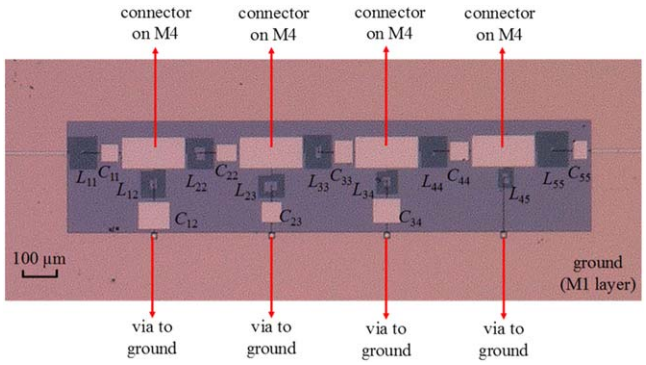

Figure 10. Micrograph of the 5th-order example. The lumped elements of every two adjacent resonators are connected by a rectangle on M4 layer.

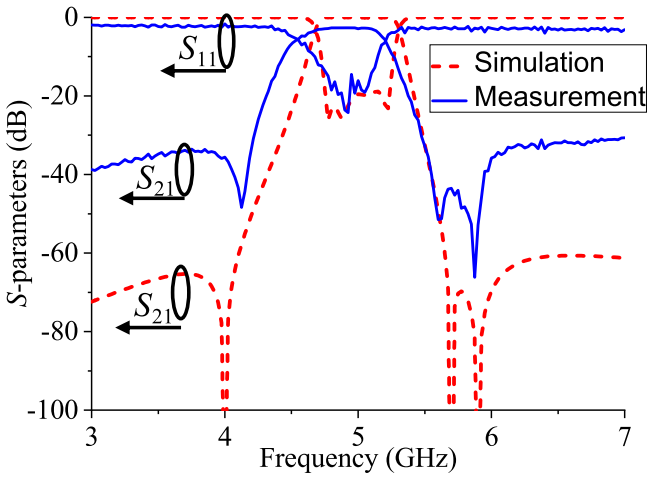

Figure 11. Simulated and tested *S*-parametrs of the 5th-order example.

Furthermore, we verify the functionality of the filter combined with an on-chip RSFQ MPG using the Josephson circuit simulator JSIM [32], whose output waveforms are illustrated in figure 12. Particularly, figure 12(a) provides the original 5 GHz MFQ pulse train generated by the MFQ driver shown in figure 1, where two SFQ pulses are generated every 200 ps. In the simulations, '0 ps' refers to the time we rise the bias voltage so that the SFQ circuit is ready for propagating SFQ pulses. By turning on the RSFQ switch at 200 ps, the SFQ pulses appear after a few picoseconds delay at around 300 ps. Note that, the amplitude of SFQ pulses, i.e. 0.45 mV, is adjustable by changing the parameter of Josephson Junctions in the RSFQ MPG for different applications. The MFQ pulse train is then converted to diverse 5-GHz microwave pulses in figures 12(b) and (c) through alternative filters (one is a lowpass filter utilized in our previous work [11], and the other is the 5th-order bandpass filter in this work). It is noticed that an output microwave with much slower rise time can be acquired when the proposed sharp-selectivity bandpass filter is applied, thus demonstrating the effectiveness of this work for quantum computing applications.

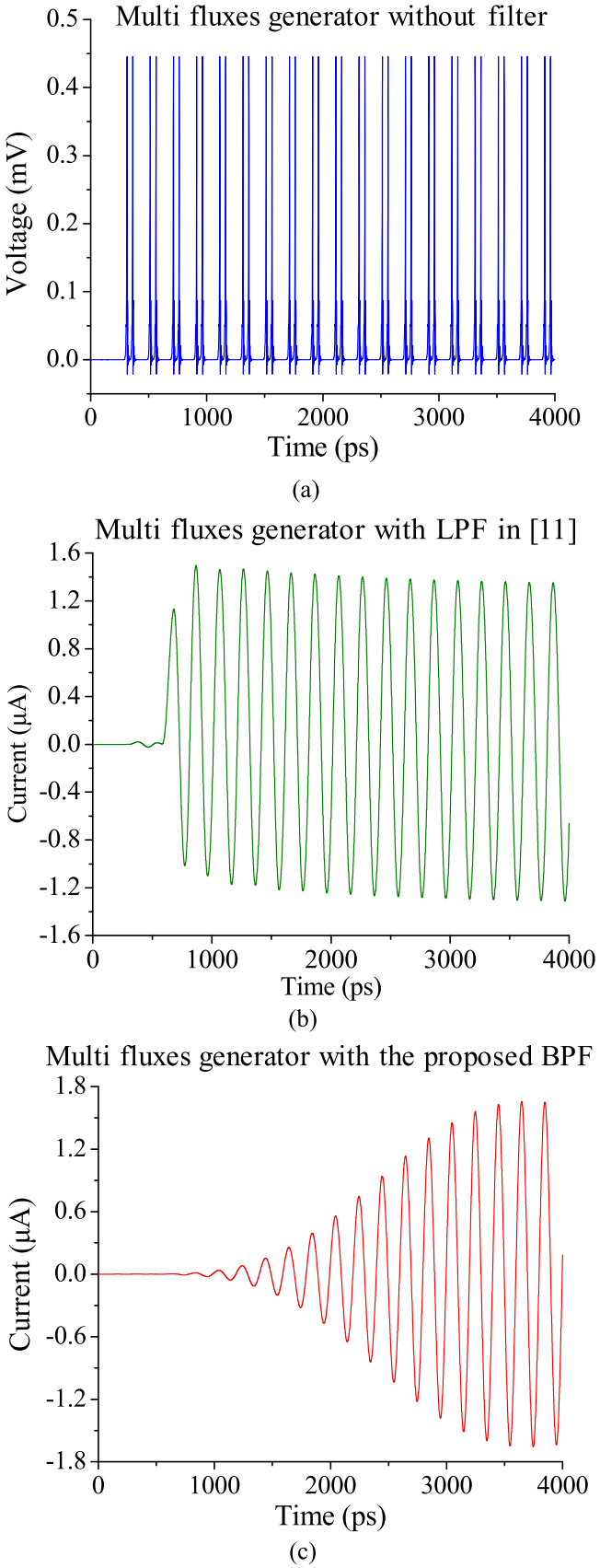

Figure 12. Simulated output waveforms of an RSFQ MPG (a) without filter, (b) with a 5th-order lowpass filter (LPF) utilized in [11], and (c) with the proposed 5th-order bandpass filter (BPF) example.

5. Conclusion

A new kind of lumped element LTS filter is proposed to achieve sharp selectivity and uneven group delay performance in this paper. Without any cross-coupling nor extra structure, multiple TZs are generated based on a group of resonant couplings individually, which results in a simple in-line topology for compact filter implementation on a chip. Complete design principles, including a direct synthesis method and a lumped circuit transformation technique, are introduced successively. Validity of the presented approach is revealed by a 5th-order example by using AIST STP2 process, where both simulated and tested results are given. In addition, the simulated output waveform by applying the filter with an RSFQ MPG is also provided, which infers the effectiveness of such filter in superconducting quantum systems in the future.

Acknowledgments

This paper is based on results obtained from a project subsidized by the New Energy and Industrial Technology Development Organization (NEDO).

ORCID iDs

Yuxing He https://orcid.org/0000-0001-5628-8080
Naoki Takeuchi https://orcid.org/0000-0003-0396-5222
Nobuyuki Yoshikawa https://orcid.org/0000-0001-6191-6715

References

[1] Liu H, Ren B, Li S and Guan X 2015 High-temperature superconducting bandpass filter using asymmetric stepped-impedance resonators with wide-stopband performance *IEEE Trans. Appl. Supercond.* **25** 1501606
[2] Sekiya N and Sugiyama S 2015 Design of miniaturized HTS dual-band bandpass filters using stub-loaded meander line resonators and their applications to tri-band bandpass filters *IEEE Trans. Appl. Supercond.* **25** 1500805
[3] Tan C, Wang Y, Yan Z, Nie X, He Y and Chen W 2019 Superconducting filter based on split-ring resonator structures *IEEE Trans. Appl. Supercond.* **29** 1500404
[4] Ren B, Ma Z, Liu H, Guan X, Wang X, Wen P and Masataka O 2019 Differential dual-band superconducting bandpass filter using multimode square ring loaded resonators with controllable bandwidths *IEEE Trans. Microw. Theory Techn.* **67** 726–37
[5] Lin Z R, Inomata K, Koshino K, Oliver W D, Nakamura Y, Tsai J S and Yamamoto T 2014 Josephson parametric phase-locked oscillator and its application to dispersive readout of superconducting qubits *Nat. Commun.* **5** 4480
[6] Sliwa K M, Hatridge M, Narla A, Shankar S, Frunzio L, Schoelkopf R J and Devoret M H 2015 Reconfigurable josephson circulator/directional amplifier *Phys. Rev.* X **5** 041020
[7] Pechal M, Besse J-C, Mondal M, Oppliger M, Gasparinetti S and Wallraff A 2016 Superconducting switch for fast on-chip routing of quantum microwave fields *Phys. Rev. Appl.* **6** 024009
[8] Naaman O, Strong J A, Ferguson D G, Egan J, Bailey N and Hinkey R T 2017 Josephson junction microwave modulators for qubit control *J. Appl. Phys.* **121** 073904
[9] Ferdinand B, Bothner D, Kleiner R and Koelle D 2019 Tunable superconducting two-chip lumped-element resonator *Phys. Rev. Appl.* **11** 034050
[10] Matsuda G, Yamanashi Y and Yoshikawa N 2007 Design of an SFQ Microwave Chopper for controlling quantum bits *IEEE Trans. Appl. Supercond.* **17** 146–9
[11] Takeuchi N, Ozawa D, Yamanashi Y and Yoshikawa N 2010 On-chip RSFQ microwave pulse generator using a multi-flux-quantum driver for controlling superconducting qubits *Physica* C **470** 1550–4
[12] Yoshikawa N 2019 Superconducting digital electronics for controlling quantum computing systems *IEICE Trans. Electron.* **E102–C** 217
[13] Lechner W, Hauke P and Zoller P 2015 A quantum annealing architecture with all-to-all connectivity from local interactions *Sci. Adv.* **1** e1500838
[14] Nigg S E, Lörch N and Tiwari R P 2017 Robust quantum optimizer with full connectivity *Sci. Adv.* **3** e1602273
[15] Puri S, Andersen C K, Grimsmo A L and Blais A 2017 Quantum annealing with all-to-all connected nonlinear oscillators *Nat. Commun.* **8** 15785
[16] Rafique R, Ohki T, Banik B, Engseth H, Linner P and Herr A 2008 Miniaturized superconducting microwave filters *Supercond. Sci. Technol.* **21** 075004
[17] Rafique R, Ohki T, Linner P and Herr A 2009 Niobium tunable microwave filter *IEEE Trans. Microw. Theory Techn.* **57** 1173–9
[18] Rafique R, Linnér P, Motlagh B M, Banik B, Ohki T and Herr A 2007 Miniaturization of superconducting passive filters for on-chip applications *The 11th Int. Superconductive Electronics Conf. (ISEC 2007) (Washington, DC)*
[19] Rafique R, Ohki T, Engseth H and Herr A 2007 RSFQ based microwave controller for qubit *The 11th Int. Superconductive Electronics Conf. (ISEC 2007) (Washington, DC)*
[20] Setoodeh S, Laforge P D and Mansour R R 2011 Realization of a highly miniaturized wideband bandpass filter at the UHF band *IEEE Trans. Appl. Supercond.* **21** 538–41
[21] Barinov A E and Zhgoon S A 2002 Planar superconducting lumped element bandpass filter with spiral inductors *Supercond. Sci. Technol.* **15** 1040
[22] Cameron R J 1999 General coupling matrix synthesis methods for Cheby-shev filtering functions *IEEE Trans. Microw. Theory Techn.* **47** 433–42
[23] Kozakowski L A, Sypek P and Mrozowski M 2005 Eigenvalue approach to synthesis of prototype filters with source/load coupling *IEEE Microw. and Wireless Compon. Lett.* **15** 98–100
[24] Tamizzzo S and Macchiarella G 2005 An analytical technique for the synthesis of cascaded N-tuplets cross-coupled resonators microwave filters using matrix rotations *IEEE Trans. Microw. Theory Techn.* **53** 1693–8
[25] He Y, Macchiarella G, Wang G, Wu W, Sun L, Wang L and Zhang R 2018 A direct matrix synthesis for in-line filters with transmission zeros generated by frequency-variant couplings *IEEE Trans. Microw. Theory Techn.* **66** 1780–9
[26] He Y, Macchiarella G, Ma Z, Sun L and Yoshikawa N 2019 Advanced direct synthesis approach for high selectivity in-line topology filters comprising N-1 adjacent frequency-variant couplings *IEEE Access* **7** 41659–68

[27] Hunter I 2001 Designs of lumped lowpass prototype networks *Theory and design of microwave filters* (United Kingdom: The Institution of Engineering and Technology) 3 (https://doi.org/10.1049/PBEW048E)

[28] Macchiarella G 2008 Generalized coupling coefficient for filters with nonresonating nodes *IEEE Microw. Wireless Compon. Lett.* **18** 773–5

[29] Park J, Lee S and Lee Y 2012 Extremely miniaturized bandpass filters based on asymmetric coupled lines with equal reactance *IEEE Trans. Microw. Theory Techn.* **60** 261–9

[30] Nagasawa S, Hashimoto Y, Numata H and Tahara S 1995 A 380 ps, 9.5 mW Josephson 4-Kbit RAM operated at a high bit yield *IEEE Trans. Appl. Supercond.* **5** 2447–52

[31] Fourie C J 2015 Full-gate verification of superconducting integrated circuit layouts with InductEx *IEEE Trans. Appl. Supercond.* **25** 1300209

[32] Fang E and Van Duzer T 1989 A josephson integrated circuit simulator (JSIM) for superconductive electronics application *The 1989 Int. Superconductivity Electronics Conf. (ISEC '89) (Tokyo)* pp 407–10